Effect of niobium doping on the properties of picosecond laser-induced transient gratings in $KTa_{1-x}Nb_xO_3$

Huimin Liu and Richard C. Powell
Center for Laser Research, Oklahoma State University, Stillwater, Oklahoma 74078

L. A. Boatner
Solid State Division, Oak Ridge National Laboratory, Oak Ridge, Tennessee 37830
(Received 26 December 1990)

A study of the properties of laser-induced transient gratings produced in $KTa_{1-x}Nb_xO_3$ crystals by picosecond-pulse, two-photon excitation was carried out with use of degenerate-four-wave-mixing techniques. The grating properties were found to depend on the Nb concentration. The diffraction efficiency of the gratings exhibited a maximum at an intermediate Nb concentration while the signal decay rate increased uniformly with x. A lattice-relaxation model was developed to explain the experimental results that includes the intrinsic lattice distortion due to the niobium ions in the normally cubic perovskite crystal and the strong electron-phonon interaction causing a lattice distortion around photoionized ions. The predictions of the theoretical model agree with the experimental data. The results of grating decay-rate measurements show that the excited states produced by two-photon laser excitation act as localized quasiparticles (excitons or polarons) having a hopping rate that increases with Nb concentration x. Strong electron-phonon coupling produces phonon-assisted, incoherent hopping migration.

I. INTRODUCTION

The results of the observation of laser-induced transient gratings in $KTaO_3$ and $KTa_{1-x}Nb_xO_3$ (KTN) crystals produced by two-photon excitation without an external electric field were recently reported.[1] The origin of the optically induced change in the refractive index was attributed to the excitation of electrons from the valence band to the conduction band and subsequent trapping of the electrons at the B^{5+} ions in ABO_3 perovskite crystals to create B^{4+} ions in the excited state. The relaxation of the excited B^{4+} ions to the ground state gives rise to the observed fluorescence. The results of fluorescence spectra and lifetime measurements further demonstrate that the gratings are due to the change in polarizability associated with the B^{4+} ions in different electronic states. This change in polarizability is related to the lattice relaxation caused by the change in the local electronic configuration of the B^{4+} ions.

A considerable amount of experimental data was previously obtained that established the presence of structural disorder in both the cubic paraelectric and the noncubic ferroelectric phase of common perovskite crystals.[2,3] In KTN crystals, the characteristics of the observed central-peak components in light-scattering experiments[4] are consistent with those expected for an order-disorder model.[5,6] In this model, at temperatures above the phase transitions, the ions of the sublattice (Ta, Nb) are displaced from central positions in the octahedron of oxygen ions to eight equivalent positions along the cubic diagonals. These results suggest that the structural disorder may be intrinsic and is related to the order-disorder nature of the phase transitions in these materials.

In recent years, one major objective in studying KTN crystals has been to investigate the origin of the cubic-tetragonal-orthorhombic-rhombohedral sequence of structural phase transitions for perovskite-type crystals. According to a lattice-dynamics soft-mode model[7,8] proposed to explain the connection between ferroelectricity and lattice dynamics in these materials, the large static dielectric constant is the result of the unusually small frequency of a long-wavelength transverse-optical (TO) phonon branch, or the so-called soft mode. This is described in terms of the well-known Lyddane-Sachs-Teller (LST) relation. A hyper-Rayleigh-scattering study[9] at low temperatures has recently revealed a wave-vector-independent, strongly temperature-dependent contribution to the signal arising from microregions of quasistatic soft-mode polarization. These regions expanded with decreasing temperature proportional to the inverse of the soft-mode frequency. The disorder-induced scattering in the paraelectric phase is attributed to the first-order scattering from the TO and TA phonon modes. A central B-ion hopping model within a multiwell potential and a long-range hopping model were developed to explain the results.[6,10] From Raman-scattering studies, the TO frequency was found to decrease with increasing Nb concentration,[11] which means that the off-center distortion increases with Nb concentration.[12]

In this paper, we use the lattice-relaxation model to explain the observed variation of the degenerate-four-wave-mixing (DFWM) signal as a function of Nb concentration in KTN crystals. The effect of niobium doping is found to increase the lattice disorder and to accelerate the excitation-transfer hopping rate in KTN crystals.

II. EXPERIMENT

The laser-induced transient gratings were written in the samples using a frequency-doubled, Q-switched, and

mode-locked $Y_3Al_5O_{12}:Nd^{3+}$ (Nd:YAG) laser as the excitation source. At 532 nm, the laser had a pulse duration of ≈ 18 ps and repetition rate of 10 Hz. The laser-beam profile was a TEM_{00} mode with an approximate Gaussian distribution in intensity. All pulses were aligned in a DFWM configuration as described in detail in Ref. 1. Note that the probe beam was brought from the back of the sample along the reverse path of one of the pump pulses, but with its polarization rotated by 90°. In this case, the first-order Bragg-diffracted signal beam maintains this polarization (see Fig. 1) and is propagating along the reverse path of the other pumped pulse. Using this DFWM configuration, the background noise was suppressed and a high signal-to-noise ratio was attained in the experiments.

The optical delay lines are computer controlled with a stepping motor driving a retroreflector and easily provide accurate pulse delays from 15 fs to 9 ns without measurable beam-path deviation. The relative delay between the two pump pulses was adjusted to be zero by monitoring the intensity of the peak of the DFWM signal of CS_2. The DFWM measurements for all KTN samples were carried out under the same experimental conditions, taking CS_2 as a standard. The measurements were conducted at room temperature unless otherwise stated.

The single-crystal samples used in these experiments were prepared at Oak Ridge National Laboratory with the niobium concentration x ranging from 0 to 0.84. Pure $KTaO_3$ crystals have a cubic ABO_3 structure and do not undergo a phase transition to a ferroelectric phase, while $KNbO_3$ undergoes a cubic-to-tetragonal phase transition at 428 °C. For mixed crystals at room temperature, a KTN ($KTa_{1-x}Nb_xOQ_3$) sample with $x=0.37$ is in the cubic phase with $T_c=20$ °C, while a KTN sample with $x=0.4$ and $T_c=40$ °C is tetragonal and shows interesting electro-optic properties[13,14] due to the large value of the dielectric susceptibility close to the transition temperature. However, the ferroelectricity can be observed only by using an external electric field with single-domain crystals. In order to exclude any influence of the electro-optic effect on the results of this study, all of the KTN samples were unpoled.

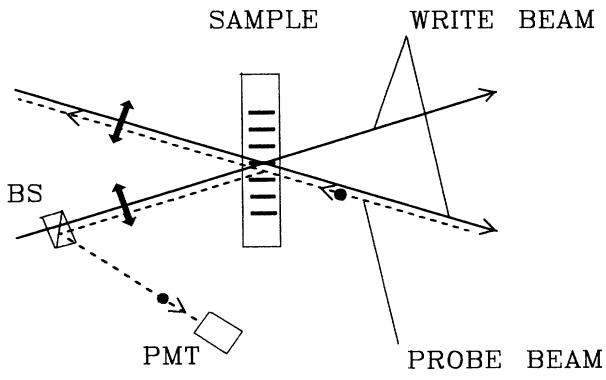

FIG. 1. Geometry and polarization orientations of the write beams, probe beam, and signal beam crossing in the sample.

III. PROPERTIES OF THE TRANSIENT GRATINGS

The properties of the two-photon-excited transient gratings were determined by monitoring the diffracted signal-beam intensity and decay time as a function of the intensity and crossing angle of the write beams. The intensity ratio of the scattered-signal beam to the incident-probe beam is defined as the absolute diffraction efficiency η. This is then normalized to a 1-mm sample thickness in order to compare samples. The absolute diffraction efficiency was found to vary with the crossing angle of the two write beams as discussed in Ref. 1. At a fixed crossing angle, absolute diffraction efficiency depends on the Nb concentration as shown in Fig. 2. The solid data points in the figure represent the measured diffraction efficiency at the write-beam crossing angle of $2\theta=10.6°$ and a total write-beam intensity of 35 mJ/cm^2. In the lower niobium concentration region, the measured value of η increases with x, while in the higher niobium concentration region it decreases with x. As pointed out in Ref. 1 this behavior may be associated with the structural variation of the crystals, which undergo a phase transition at room temperature at approximately the same value of x that gives the maximum DFWM scattering efficiency. The physical origin of this effect is attributed to the presence of the intrinsic lattice distortion due to the niobium dopant ion, as will be discussed below.

The grating scattering signals of all of the KTN samples exhibit nearly exponential decay patterns. Figure 3 shows a grating decay curve for the signal from the $KTa_{1-x}Nb_xO_3$ sample with $x=0.62$, which was obtained by scanning the probe beam from negative delay to ≈ 8 ns. A rise time from zero-delay to the signal maximum, as shown in the inset of the figure, was found to exist for all of the samples. It was in the range of 10–100 ps depending on the sample and the crossing angle of the

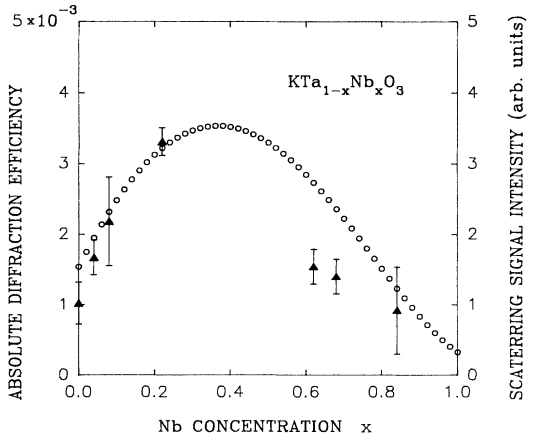

FIG. 2. Maximum DFWM diffraction efficiency of the mixed KTN crystals vs Nb concentration x. The solid data points represent the measured absolute diffraction efficiency corresponding to the left-hand-side coordinate, while the open data points represent the theoretical prediction corresponding to the right-hand-side coordinate. The measurements were conducted at a write-beam crossing angle of $2\theta=10.6°$ and total write-beam intensity of 35 mJ/cm^2.

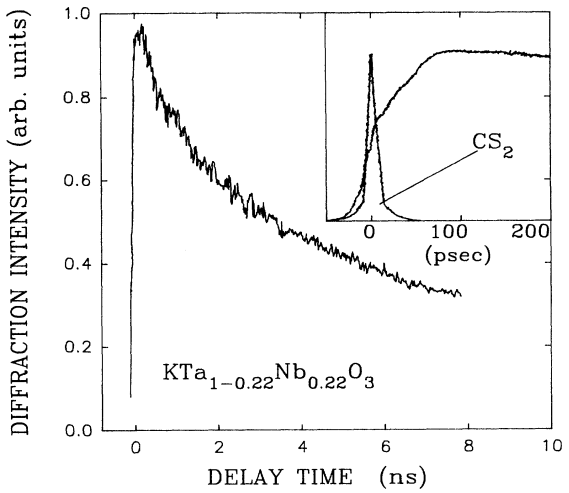

FIG. 3. DFWM signal decay pattern of KTN, a crystal with $x=0.22$. The inset shows the signal buildup at time $t>0$, reaching the maximum at $t=80$ ps.

two write beams.

The transient-grating decay rate was measured as a function of the Nb concentration and of the crossing angle of the two write beams. At a fixed crossing angle, the decay rate monotonically increases with niobium concentration. Figure 4 shows typical results obtained on $KTa_{1-x}Nb_xO_3$ samples at a crossing angle of $2\theta=41.3°$. At a specific niobium concentration x, on the other hand, the decay rate increases with the crossing angle. Figure 5 shows the decay rates versus $1/\Lambda^2$ for the $KTa_{0.96}Nb_{0.04}O_3$ and $KTa_{0.78}Nb_{0.22}O_3$ samples. Λ is the grating spacing and is related to the write-beam crossing angle θ through the expression $\Lambda=\lambda/2\sin\theta$. Extrapolating the results to $1/\Lambda=0$ yields a decay rate equal to $2/\tau$, where τ is the luminescence lifetime. The slope of the decay rate versus $1/\Lambda^2$ curves increases with x as

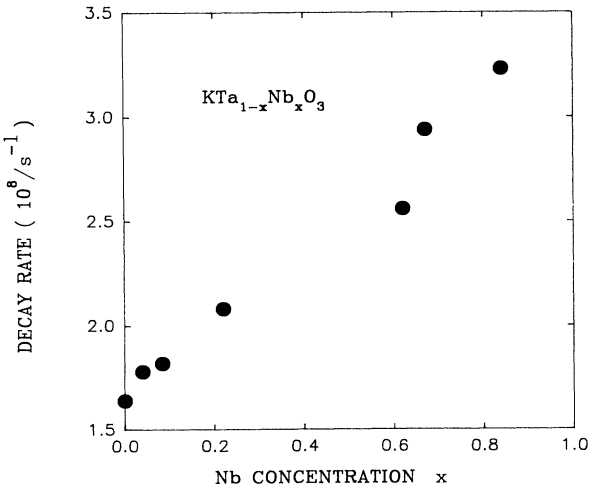

FIG. 4. Transient-grating decay rate of KTN crystals as a function of Nb concentration x. The measurements were taken at a crossing angle of the two write beams of $2\theta=41.3°$.

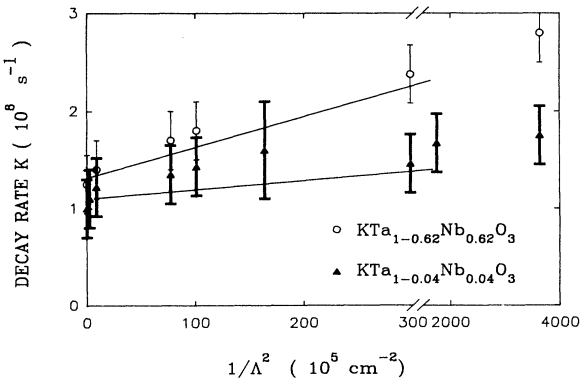

FIG. 5. Grating decay rate vs $1/\Lambda^2$ for $KTa_{1-0.04}Nb_{0.04}O_3$ and $KTa_{1-0.62}Nb_{0.62}O_3$ crystals. The data points at $1/\Lambda^2=0$ represent twice the fluorescence decay rates.

seen in Fig. 6. The slope is given by $q=\Delta K/\Delta(1/\Lambda^2)$, where K is the decay rate.

The decay rate of the transient grating increases when the KTN crystal is doped with impurity ions. Figure 7 shows the grating decay curves for 0.06-wt% Ni_2O_3-doped and -undoped $KTaO_3$ crystals. Doped $KTaO_3(1)$ represents an untreated sample, where the dopants are mainly in the form of Ni^{3+} ions.[1,15] Doped $KTaO_3(2)$ represents a sample annealed under a strongly reducing atmosphere at 900 °C for a few hours, where Ni^{2+} ions are the dominant species. From the undoped $KTaO_3$ sample to the doped $KTaO_3(2)$ sample, the grating decay rate increases significantly. The measured decay rates for the $KTaO_3(1)$ and $KTaO_3(2)$ samples are plotted versus $1/\Lambda^2$ in Fig. 8 The slope of the curves is greater for the treated sample and the slopes of the curves for the doped samples are an order of magnitude greater than that of the undoped sample.

IV. INTERPRETATION OF THE EXPERIMENTAL RESULTS

The two important experimental results to be explained are the variations of the DFWM signal strength and de-

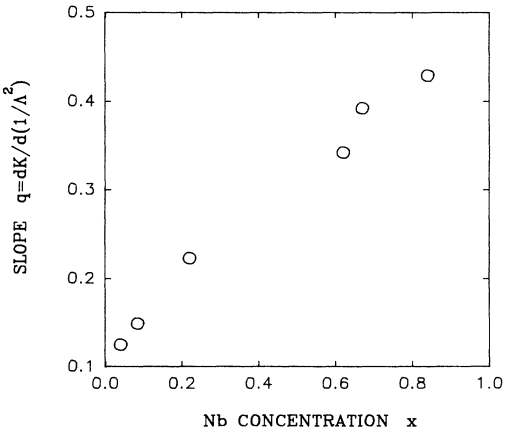

FIG. 6. The slope measured from plotting the grating decay rates vs grating spacing for KTN samples with different Nb concentrations x.

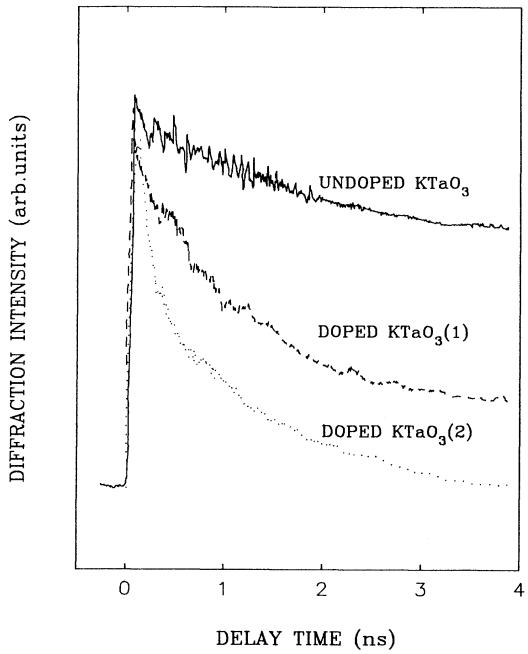

FIG. 7. The grating signal decay curves for undoped $KTaO_3$ crystal and 0.06-wt. % Ni_2O_3-doped $KTaO_3$ crystals. Doped $KTaO_3$(1) represents an untreated sample while doped $KTaO_3$(2) represents a sample heat treated under a strong reducing atmosphere at 900 °C for a few hours.

cay rate as a function of niobium concentration. Several other observations are important in understanding these results. In previous research on the luminescence properties of KTN crystals,[1] the experimental results showed a strong interaction between the luminescent B^{4+} ions and the lattice resulting in a large lattice relaxation around these ions. Also, inelastic-scattering studies have shown that the TO vibrational mode frequency decreases with

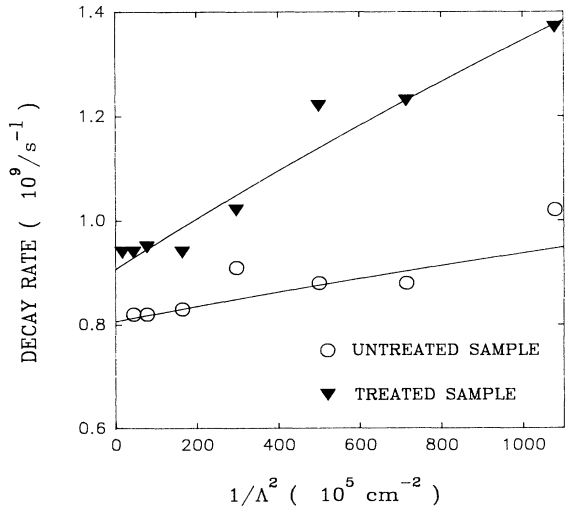

FIG. 8. Grating signal decay rate vs $1/\Lambda^2$ for the 0.06-wt. % Ni_2O_3-doped $KTaO_3$ crystals.

Nb concentration,[11] which indicates an increase in the intrinsic lattice distortion. In addition, the dynamical properties of the transient gratings seen in Figs. 3–5 are found to be correlated with the luminescence decay properties. Based on this information, a lattice-relaxation model is developed below to interpret the variation of the DFWM signal properties with Nb concentration. The theory of lattice relaxation was developed several decades ago,[16,17] and is still of current interest in the area of spectroscopy of solids, although theoretical complexity often restricts its application.

A. Lattice-relaxation model

To begin with, the correlation between radiationless relaxation processes of luminescent centers and the lattice relaxation is summarized. The experimental data obtained from luminescence measurements can be used to estimate the magnitude of the lattice relaxation. The electrons of a luminescent center in a solid interact with the electrons of the surrounding lattice atoms. This interaction causes the relative equilibrium positions of the lattice atoms to be displaced when the central ion changes its electronic state (for example, the initial ground state and the final excited state). This ion displacement or lattice distortion depends upon the electronic state of the central ion and is referred to as the lattice relaxation.

For the sake of simplicity, a double-potential-well configuration coordinate system which represents the initial state $|i\rangle$ and final state $|f\rangle$ of the system is assumed. The total Hamiltonian

$$H = H_e + H_{eL} + H_L \tag{1}$$

is a sum of the electronic H_e, electron-phonon interaction H_{eL}, and lattice vibration H_L Hamiltonians. In the adiabatic approximation, the total wave function of the system in the initial state is

$$\Psi_{i,n'}(x,R) = \Phi_i(x,R)\chi_{in'}(R) \ . \tag{2}$$

This is a product of the electronic part $\Phi_i(x,R)$ and the lattice vibration part $\chi_{in'}(R)$ of the wave function, and x and R are the coordinates of the electrons and ions, respectively. Within the framework of the Condon approximation, a multiphonon, radiationless transition process has a probability

$$w_{\text{non}} = (2\pi/\hbar)\text{Av}_n \left[\sum_{n'} |\langle in'|H|fn\rangle|^2 \delta(E_{in'} - E_{fn}) \right] , \tag{3}$$

where the matrix element is

$$\langle in'|H|fn\rangle = \int\int \Phi_i(x,R)\chi_{in'}(r) H \Phi_f(x,R)\chi_{fn}(R)dx\,dR \ . \tag{4}$$

The electronic wave function $\Phi_i(x,R)$ in Eq. (4) is a first-order perturbed wave function given by

$$\Phi_i(x,R) = \Phi_i^0(x) + \sum_k \frac{\langle k|H_{eL}|i\rangle}{E_i^0 - E_k^0} \Phi_k^0(x) \ , \tag{5}$$

where $\Phi^0(x)$ is the zeroth-order eigenfunction of H_e, and H_{eL} is assumed to be linear in terms of lattice displacement.

Equation (3) involves averaging over all phonon states. In the limit of high temperature and strong electron-phonon coupling, the nonradiative transition probability is reduced to[18]

$$w_{\text{non}}=(1/\hbar)\sqrt{\pi kT/S\hbar\omega}M_{if}\exp\left[\frac{-(E_{if}-S\hbar\omega)^2}{4kTS\hbar\omega}\right], \tag{6}$$

where the matrix element M_{if} involves only the electronic part. The parameters S, $\hbar\omega$, E_{if} are expressed in Fig. 9 and have been determined in Ref. 1. The activation energy ΔE is

$$\Delta E=\frac{(E^{if}-S\hbar\omega)^2}{4S\hbar\omega}. \tag{7}$$

The fluorescence decay rate can be written as

$$1/\tau=w_{\text{radiative}}+w_{\text{nonradiative}}, \tag{8}$$

where the radiative transition probability $w_{\text{radiative}}$ is assumed to be temperature independent and can be determined using the luminescence data obtained at 5 K (Refs. 19 and 20) where $w_{\text{nonradiative}}\rightarrow 0$. Assuming that the radiationless decay process occurs at point C in Fig. 9, Eqs. (6)–(8) show the correlation between $S\hbar\omega$ and the luminescence lifetime and how this parameter can be determined through the temperature dependence of the fluorescence lifetime. Figure 10 shows the values obtained for $S\hbar\omega$ as a function of the luminescence lifetime obtained in the mixed $KTa_{1-x}Nb_xO_3$ crystals[1] using this model.

The lattice-relaxation properties can now be determined using the values obtained for $S\hbar\omega$. In a harmonic approximation, the configurational-coordinate potential well can be expressed as

$$E_2=E_f+\tfrac{1}{2}\omega_s^2R^2 \tag{9}$$

for the final state $|f\rangle$, and

$$E_1=E_i+\tfrac{1}{2}\omega_s^2(R+\Delta_{if})^2 \tag{10}$$

for the initial state $|i\rangle$. A linear approximation assuming the same force constants ω_s for two potentials has been employed. The position of the crossing point C is given by

$$R_C=\frac{E_{if}-\frac{1}{2}\omega_s^2\Delta_{if}}{\omega_s^2\Delta_{if}}. \tag{11}$$

Also,

$$\Delta E=\tfrac{1}{2}\omega_s^2R_C^2=\frac{(E_{if}-\frac{1}{2}\omega_s^2\Delta_{if}^2)^2}{2\omega_s^2\Delta_{if}^2}. \tag{12}$$

Comparing Eq. (12) to Eq. (7) gives

$$S\hbar\bar{\omega}=\tfrac{1}{2}\bar{\omega}_s^2\Delta_{if}^2. \tag{13}$$

The lattice displacement or the temporary lattice distortion Δ_{if} can thus be determined from the values obtained for $S\hbar\omega$.

B. Origin of the polarization change

In the limit of small displacements, the polarizability of a polar molecule is[21,22]

$$\alpha=r^3/\xi+1, \tag{14}$$

where r is the distance between cation and anion and ξ is a crystal-dependent parameter. The change in polarizability due to a displacement Δr is therefore

$$\Delta\alpha=(3r^2/\xi+1)\Delta r. \tag{15}$$

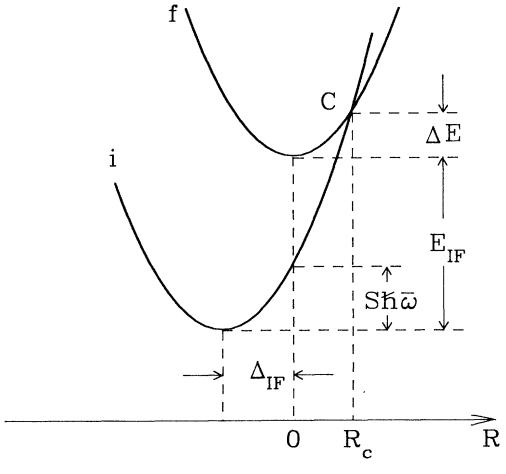

FIG. 9. Double-potential-well configuration coordinate model for the lattice-relaxation model. The lower parabola represents the B^{4+} ground state while the upper parabola represents the B^{4+} excited state. The abscissa R represents the lattice coordinate. All terms are defined in the text.

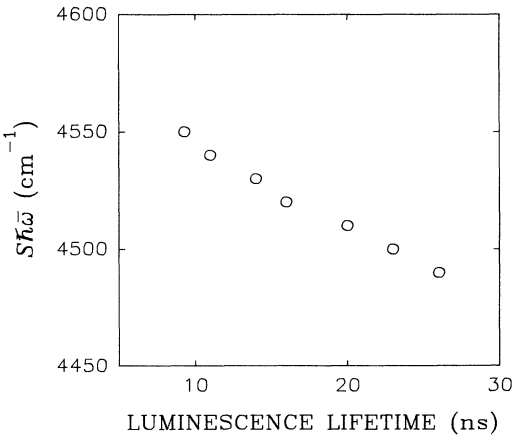

FIG. 10. Values of $S\bar{\hbar}\omega$ vs luminescence lifetime in $KTa_{1-x}Nb_xO_3$ crystals.

Assuming that the ionic displacement due to electronic excitation corresponds to the lattice relaxation Δ_{if}, the change in polarizability can be related to the values obtained for $S\hbar\omega$. However, two factors that affect the polarizability change $\Delta\alpha$ must be taken into account. One is the mean interionic distance r in the $KTa_{1-x}Nb_xO_3$ crystals, which varies with niobium concentration x. The other is the presence of the intrinsic off-center displacement due to the addition of niobium ions. The results of inelastic-scattering studies[11,12] can be used to estimated the off-center displacement. Crystallographic data give the dimensions of the unit cell in different directions.[23]

It is important to note that the lattice relaxation depends only on the electronic configurations of the initial state and the final state. The net interionic displacement can be determined with the intrinsic part subtracted. For the sake of simplicity, all the parameters in this model are assumed to vary linearly with the niobium concentration x. These are given by the mean interionic distance

$$r = r_{KTaO_3} + \beta_1 x \ , \tag{16}$$

the intrinsic displacement

$$\Delta_{intr} = \beta_2 x \ , \tag{17}$$

the change in $S\hbar\omega$,

$$\Delta(S\hbar\bar{\omega}) = \beta_3 x \ , \tag{18}$$

and the effective mass of the B^{5+}-O group

$$M = (M_{Ta} + M_O + \beta_4 x)/2N_0 \ , \tag{19}$$

where N_0 is Avogardro's constant. Using these definitions in Eq. (15), the total polarizability is given by

$$\Delta\alpha = \zeta(r_{KTaO_3} + \beta_1 x)^2[\sqrt{2(S\hbar\omega + \beta_3 x)}/\omega_s^2 - \beta_2 x] \ , \tag{20}$$

where ζ is a lattice-related coefficient and $\omega_s^2 = M\omega^2$.

Under two-photon excitation, the diffraction efficiency of a laser-induced transient grating η can be expressed as[1]

$$\eta_{max} = \left[\frac{\Delta\alpha\pi d N}{2n\lambda\cos\theta} \frac{\sigma_\beta I^2}{(h\nu)^2} \delta t \right]^2 \ , \tag{21}$$

where η_{max} is the maximum absolute diffraction efficiency and σ_β is the two-photon absorption cross section of the KTN crystal. I and δt are the laser intensity and the laser pulse duration, respectively, 2θ is the crossing angle of the two write beams, N is the total population density, d is the grating thickness, and $h\nu$ is the photon energy of the pump source. Inserting Eq. (20) into Eq. (21) yields

$$\eta_{max} = f(\theta, n, \xi, I, d, \lambda, \delta t)(r_{KTaO_3} + \beta_1 x)^4 \times [\sqrt{2(S\hbar\omega + \beta_3 x)}/\omega_s^2 - \beta_2 x]^2 \ , \tag{22}$$

where f is a function of all the variables shown enclosed in the parentheses.

Plotting the absolute diffraction efficiency versus niobium concentration gives a good fit between the measured experimental results and the predictions of Eq. (22) as shown in Fig. 2. The measurements of the absolute diffraction efficiency were sensitive to the crystal quality. In Fig. 2 the data points with large error bars are due to samples with poor crystal quality. The parameters used in the theoretical analysis are listed in Tables I and II. Note that only one parameter ω was properly adjusted from 1.27×10^{13} s^{-1}, (which was taken as the mean phonon frequency in the calculation) to 1.04×10^{13} s^{-1}. The good theoretical fit to the data shows that the physical origin of the variation of the DFWM signal intensity with niobium concentration can be attributed to the presence of the intrinsic disorder when niobium ions are present. In addition, the lattice-relaxation model is shown to be a good theoretical means for characterizing some of the important properties of photorefractive materials.

C. Excitation migration

As shown in Fig. 4, all of the transient-grating decay times are in the range of 10^{-9}–10^{-8} s, which is the same range as the luminescence lifetimes. Thus, in the time region of interest, the dynamical processes affecting the properties of the transient gratings appear to be associated with the dynamical processes affecting the luminescent centers. One important type of process is nonradiative excitation migration. This can take place by mobile quasiparticles such as Frenkle excitons or small polarons. The data obtained here cannot directly distinguish between these two types of quasiparticles. For either case, a diffusion model can be employed to describe this process. In this model the grating signal decay rate K is expressed as[24]

$$K = 2\{[(\phi + 1/\tau)^2 + (4\pi V a/\Lambda)^2]^{1/2} - \phi\} \ , \tag{23}$$

where τ is the fluorescence lifetime, a is the distance between two B ions, V is the ion-ion interaction rate, and ϕ is the excitation scattering rate. As pointed in Ref. 24, under conditions for which the excitation migration is incoherent, the expression for the grating decay rate reduces to

$$K = 2/\tau + (8\pi^2/\Lambda^2)D \ , \tag{24}$$

where D is the diffusion coefficient. Using Eq. (24), the values of D can be determined from the slopes of the lines shown in Fig. 5. The measured diffusion coefficients for $KTa_{1-x}Nb_xO_3$ samples with different values of x are plotted in Fig. 11. The effect of the niobium ions appears to be an enhancement of the excitation transfer.

The lattice-relaxation model developed above to analyze the DFWM diffraction efficiency results can also be employed to interpret the excitation migration data. The presence of strong electron-phonon coupling results in localization of the excitation at a lattice site. This mobile excitation can be treated either as a Frenkel exciton or a small polaron that migrates from one lattice site to another carrying with it the local lattice distortion.[25,26]

TABLE I. Linear coefficients and phonon frequency.

β_1 (Å)	β_2 (Å)	β_3 (cm^{-1})	β_4	$\bar{\omega}$ (s^{-1})
0.86	0.88	50	−88	1.04×10^{13}

TABLE II. Parameters used to determine the linear coefficients.

	$KTaO_3$	$KNbO_3$
Mean *B*-O interionic distance (Ref. 23) (Å)	1.99	2.85
$S\hbar\bar{\omega}$ (cm^{-1})	4490	4550
Force constant $\bar{\omega}_s^2$ ($10^4\times cm^{-1}/Å^2$)	1.32	0.73
Δ_{max} (Å)	0.82	1.11
Effective mass (10^{-24} g)	1.63	0.90
Intrinsic off-center distortion (Ref. 23) (Å)	0	0.88

From the results of small polaron theory,[25] it is known that the excitation motion in this limiting case is a series of uncorrelated hops and can be described as a random walk over the lattice sites.[25] The expression for the diffusion coefficient due to incoherent hopping was derived by Munn, *et al.*[27] including terms that are quadratic with respect to displacement in the Hamiltonian for the electron-phonon interaction. The result is

$$D=(\pi a^2 M\rho/\hbar)[\exp(-\hbar\omega/kT)/1+\exp(-\hbar\omega/kT)] . \quad (25)$$

Here a is the mean free path, M is the matrix element of the resonance interaction resulting in a hop of an excitation to a neighboring site in the rigid lattice $\rho=2M/\Gamma$, and Γ is the phonon bandwidth. At high temperatures, the diffusion coefficient increases exponentially with increasing temperature as in the phonon-assisted excitation migration theory of Trlifaj.[28] However, in this case, nonresonant excitation gives rise to a high density of phonons in the region around the excited ion due to radiationless relaxation processes. Due to this nonequilibrium phonon distribution, the diffusion coefficient obtained from these experiments may be orders-of-magnitude larger than that estimated from the theoretical expression based on a thermal phonon distribution.

To characterize the excitation hopping rate, Eq. (25) can be rewritten in simplified form as

$$D=a^2\nu , \quad (26)$$

where ν is defined as the frequency of hops so that $1/\nu$ is the mean hopping time. Assuming that the interaction causing the diffusion is dipole-dipole in nature, the excitation transfer rate is proportional to the reciprocal of the sixth power of the interionic distance[29] a and, hence, the diffusion coefficient will be given by[26]

$$D=C/a^4 , \quad (27)$$

where C is a constant describing the strength of the interaction. In the case of pure $KTaO_3$ or $KNbO_3$ crystals, the constant C is associated with the exciton hopping on the lattice of tantalate or niobate molecular ions, respectively. Neglecting the effect of cross hopping between the two types of molecular ions, the total diffusion coefficient D can be expressed as

$$D=D_{Ta}(1-x)^{4/3}+D_{Nb}x^{4/3} , \quad (28)$$

where D_{Ta} and D_{Nb} are the diffusion coefficients for pure $KTaO_3$ and pure $KNbO_3$ crystals, respectively. In Fig. 11 the predictions of this expression are shown to give a good fit to the experimental results. The diffusion coefficients obtained from this fit are $D_{Ta}=1.8\times10^{-3}$ cm^2/s and $D_{Nb}=7.3\times10^{-3}$ cm^2/s. This indicates that the strength of the interaction causing the migration is larger for the niobium lattice than for the tantalum lattice, hence $\nu_{Nb}>\nu_{Ta}$.

Taking[25] $a=2r$, the theoretical predictions of Eqs. (26)–(28) for hopping rate ν versus x are plotted in Fig. 12. It is in good agreement with the experimental obser-

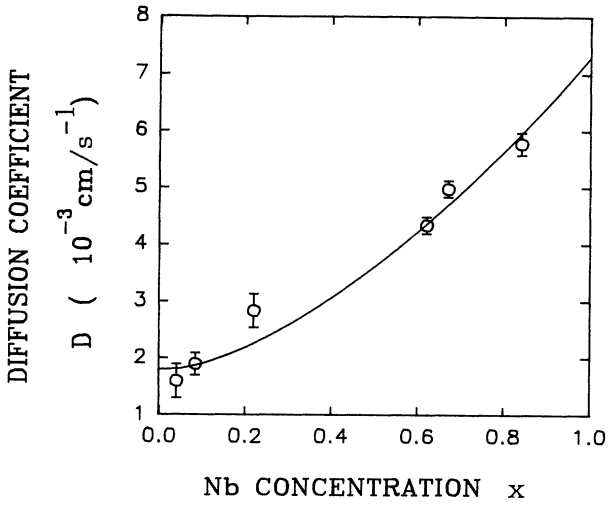

FIG. 11. Measured diffusion coefficient D in $KTa_{1-x}Nb_xO_3$ crystals with different niobium concentrations. The solid line represents the best fit of Eq. (27).

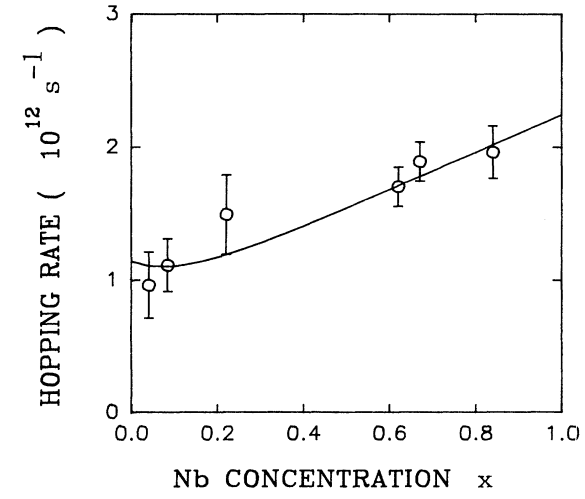

FIG. 12. Exciton hopping rate vs Nb concentration x. Theoretical predictions (solid curve), observed values (open points).

TABLE III. The measured mean hopping time of the excitons in $KTa_{1-x}Nb_xO_3$ crystals with different niobium concentrations.

	Nb concentration					
(x)	0.04	0.084	0.22	0.62	0.67	0.84
	Hopping time					
(ps)	1.04	0.90	0.67	0.59	0.53	0.51

vations. Table III shows the measured mean hopping time versus x. All these experimental results and the theoretical predictions show that the excitation hopping in $KTa_{1-x}Nb_xO_3$ mixed crystals is enhanced with niobium doping.

The impurity ions doped into the sample appear to increase the nonradiative decay rate and the excitation diffusion coefficient as shown in Fig. 8. The measured values of D are an order of magnitude larger than those found for the undoped sample, and the value of D doubled after heat treatment.

These results can be correlated with those obtained from the fluorescence lifetime measurements. The increase in the fluorescence decay rates of the doped $KTaO_3(1)$to $KTaO_3(2)$ samples is due to the increase in trap concentration. As mentioned in Sec. III, in the $KTaO_3(2)$ sample, Ni^{2+} ions are predominant. Under laser excitation, photoionization results in $Ni^{2+}+h\nu \rightarrow Ni^{3+}+e$, which increases the concentrations of both free electrons and traps. The former gives rise to an increase in the DFWM signal intensity[1] while the latter accelerates the grating decay. In addition, the presence of these defects in multivalence states can give rise to donor-acceptor pair energy transfer.[29] The long-range, single-step, and free-electron migration processes related to doping ions can result in a faster smoothing of the spatial grating pattern than that produced by phonon-assisted excitation hopping.

V. DISCUSSION

The origin of the DFWM signals produced by picosecond-pulse, two-photon absorption was identified in Ref. 1 as being associated with the creation of Nb^{4+} or Ta^{4+} ions. The presence of lattice relaxation was found to be important in explaining the optical properties and the magnitude of the DFWM signal in these samples. In the present paper, this investigation has been extended to determine the effects of Nb ions on the properties of KTN crystals and to determine the mobility of the excited states that are created. The lattice-relaxation model has been extended to interpret these results.

The observed effects of niobium ions on the properties of transient gratings induced by two-photon excitation of KTN crystals are consistent with the lattice-relaxation model developed previously. The real system is more complex than the model developed here. For example, the real system has a continuous distribution of phonon modes instead of a single mode as used in the model. Furthermore, all terms in Eqs.(16)–(19) are assumed to be linear functions of niobium concentration x. This is valid for the intrinsic lattice distortion term according to the experimental results obtained from inelastic-scattering studies.[11,12] For the other terms, however, the exact forms of the functional dependences are not known. The parameters used in the theoretical fit were taken from different experimental results, except for one parameter, $\hbar\omega$, that was adjusted to give a good fit to the data. The agreement between the theoretical prediction and experimental results of the variation of the DFWM signal intensity versus Nb concentration indicates the qualitative validity of the physical fundamentals of this model. This shows that DFWM results are consistent with the results of the inelastic-scattering measurements, both of which demonstrate the effects of the structural deformation of KTN crystals. However, the exact values of some of the parameters obtained from the quantitative use of this model may not be realistic because of the simplifying assumptions. For example, the activation energy ΔE described here as a barrier for nonradiative processes appears to be too high, and the real excitation process of the crystal should be described by a multiwell system instead of the two-well configuration. In addition, processes not included in this simple model, such as nonradiative tunneling between two potential wells,[29] may be important.

The results of the analysis of the dynamical properties of the DFWM signals were also consistent with the lattice-relaxation model. The laser excitation produces excited states of the niobate or tantalate molecular ions that make up sublattices in KTN crystals. The strong electron-phonon interaction producing the lattice relaxation results in incoherent excitation hopping from ion to ion on these sublattices which is enhanced by high local phonon densities. When the electron and hole localized on the same molecular ion move together, this is a Frenkle exciton. When the electron moves without the hole, this is a small polaron. The data cannot directly distinguish between these two cases. However, the fact that postulating a dipole-dipole interaction for the hopping mechanism gives an excellent fit to the observed concentration dependence for ν and D is consistent with exciton migration. The enhanced diffusion observed in Ni-doped samples may reflect the additional contribution to the excitation migration associated with polarons due to the presence of additional charges produced by the doping ions. The data indicate that the interaction causing the hopping is stronger for niobate ions than for tantalate ions, which, in this model, implies a stronger electron-phonon coupling for the former. This is consistent with the fluorescence lifetime observations that show a greater radiationless decay rate for the niobate ions than for the

tantalate ions.

In conclusion, the lattice-relaxation model developed to explain the results of DFWM measurements provides an enhanced understanding of the effects of Nb ions on the optical and structural properties of displacive ferroelectric crystals such as KTN. One important observation that is not yet fully understood involves the origin of the fast DFWM signal observed in $KNbO_3$ crystals.[30] The origin of this signal component is currently being investigated.

ACKNOWLEDGMENTS

The Oklahoma State University (OSU) part of this research was supported by the U. S. Army Research Office and the National Science Foundation under Grant No. DMR 87-22350. The Oak Ridge National Laboratory (ORNL) part of this research was supported by the Division of Material Sciences of the U. S. Department of Energy under Contract No. DE AC0584OR21400 with Martin Marietta Energy Systems, Inc.

[1]H. Liu, R. C. Powell, and L. A. Boatner, J. Appl. Phys. **70**, 1 (1991).
[2]G. Burns and F. H. Dacol, Solid State Commun. **42**, 9 (1982).
[3]A. M. Ouittet, M. I. Bell, M. Krauzman, and P. M. Raccah, Phys. Rev. B **14**, 5068 (1976).
[4]L. L. Chase, J. Sokoloff, and L. A. Boatner, Solid State Commun. **55**, 451 (1985).
[5]A. S. Chaves, F. C. S. Barreto, and R. A. Nogueira, Phys. Rev. B **13**, 207 (1976).
[6]J. P. Sokoloff, L. L. Chase, and D. Rytz, Phys. Rev. B **38**, 597 (1988).
[7]W. Cochran, Adv. Phys. **9**, 387 (1960).
[8]R. A. Cowley, Phys. Rev. **134A**, 981 (1964).
[9]H. Vogt, Phys. Rev. B **41**, 1184 (1990).
[10]R. A. Mullen and R. W. Hellwarth, J. Appl. Phys. **58**, 40 (1985).
[11]R. L. Prater, L. L. Chase, and L. A. Boatner, Phys. Rev. B **23**, 221 (1981).
[12]G. A. Samara, Phys. Rev. Lett. **53**, 298 (1984).
[13]F. S. Chen, J. E. Gesic, S. K. Kurtz, J. G. Skinner, and S. H. Wemple, J. Appl. Phys. **37**, 388 (1966).
[14]D. von der Linde, A. M. Glass, and K. F. Redgers, Appl. Phys. Lett. **26**, 22 (1975).
[15]M. M. Abraham, L. A. Boatner, D. N. Olson, and U. T. Hochli, J. Chem. Phys. **81**, 2528 (1981).
[16]S. E. Pekar, Zh. Eksp. Teor. Fiz. **20**, 510 (1950).
[17]K. Huang and A. Rhys, Proc. R. Soc. London, Ser. A **204**, 406 (1950).
[18]R. Kubo and Y. Toyozawa, Prog. Theor. Phys. **13**, 160 (1955).
[19]D. M. Krol, G. Blasse, and R. C. Powell, J. Chem. Phys. **73**, 163 (1980).
[20]R. C. Powell and E. E. Freed, J. Chem. Phys. **70**, 4681 (1979).
[21]A. J. Dekker, *Solid State Physics* (Prentice-Hall, Englewood Cliffs, NJ, 1957).
[22]H. Frohlich, *Theory of Dielectrics,* 2nd ed. (Oxford University, Oxford, 1958).
[23]P. Vousden, Acta Crystallogr. **4**, 373 (1951).
[24]R. C. Powell, J. K. Tyminski, A. M. Ghazzawi, and C. M. Lawson, IEEE J. Quantum Electron. **QE-22**, 1355 (1986).
[25]V. M. Agranovich and M. D. Galanin, *Electronic Excitation Energy Transfer in Condensed Matter* (North-Holland, New York, 1982).
[26]R. C. Powel and G. Blasse, Struct. Bonding (Berlin) **42**, 43 (1980).
[27]R. W. Munn and W. Siebrand, J. Chem. Phys. **52**, 47 (1970).
[28]M. Trlifaj, Czech. J. Phys. **13**, 644 (1963).
[29]T. Forster, in *Modern Quantum Chemistry,* edited by O. Sinanoglu (Academic, New York, 1966), Part III, p. 93.
[30]R. J. Reeves, M. G. Jani, B. Jassemnejad, R. C. Powell, G. J. Mizell, and W. Fay, Phys. Rev. B **43**, 71 (1991).